

Journal Pre-proof

Interfacial Effect of Pd supported on Mesoporous Oxide for Catalytic Furfural Hydrogenation

Hojeong Lee, Chinh Nguyen-Huy, Eun Jeong Jang, Jihyeon Lee, Euseob Yang, Man Sig Lee, Ja Hun Kwak, Kwangjin An



PII: S0920-5861(20)30094-8
DOI: <https://doi.org/10.1016/j.cattod.2020.02.035>
Reference: CATTOD 12703

To appear in: *Catalysis Today*

Received Date: 18 November 2019
Revised Date: 6 February 2020
Accepted Date: 24 February 2020

Please cite this article as: Lee H, Nguyen-Huy C, Jeong Jang E, Lee J, Yang E, Lee MS, Kwak JH, An K, Interfacial Effect of Pd supported on Mesoporous Oxide for Catalytic Furfural Hydrogenation, *Catalysis Today* (2020), doi: <https://doi.org/10.1016/j.cattod.2020.02.035>

This is a PDF file of an article that has undergone enhancements after acceptance, such as the addition of a cover page and metadata, and formatting for readability, but it is not yet the definitive version of record. This version will undergo additional copyediting, typesetting and review before it is published in its final form, but we are providing this version to give early visibility of the article. Please note that, during the production process, errors may be discovered which could affect the content, and all legal disclaimers that apply to the journal pertain.

© 2020 Published by Elsevier.

Interfacial Effect of Pd supported on Mesoporous Oxide for Catalytic Furfural Hydrogenation

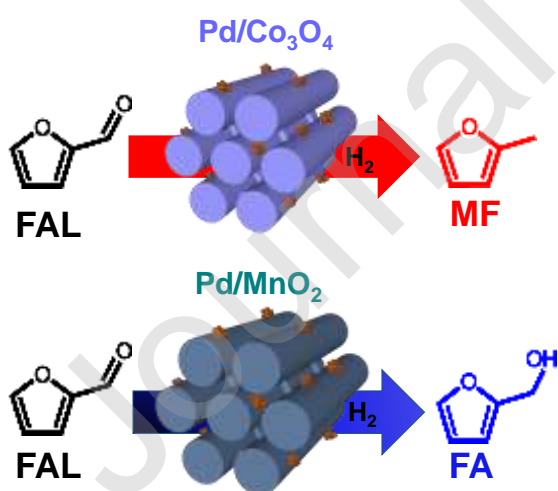
Hojeong Lee,^a Chinh Nguyen-Huy,^a Eun Jeong Jang,^a Jihyeon Lee,^a Euiseob Yang,^a Man Sig Lee,^b Ja Hun Kwak,^a and Kwangjin An^{a,*}

^aSchool of Energy and Chemical Engineering, Ulsan National Institute of Science and Technology (UNIST), Ulsan 44919, Republic of Korea

^bKorea Institute of Industrial Technology (KITECH), Ulsan 44413, Republic of Korea

* Corresponding author (E-mail: kjan@unist.ac.kr)

Table of Contents



Highlights

- Pd nanoparticles are homogeneously dispersed to mesoporous oxides.
- Pd/oxide catalysts enhance catalytic conversions of furfural.
- Pd/Co₃O₄ catalyst shows enhanced conversion in furfural hydrogenation.
- Furfural is converted via either aldehyde hydrogenation or hydrogenolysis.
- 2-methylfuran is selectively produced over Pd/Co₃O₄ catalyst via hydrogenolysis.

Abstract

Highly dispersed Pd is loaded onto different types of mesoporous oxide supports to investigate the synergetic metal-support effect in catalytic furfural (FAL) hydrogenation. Ordered mesoporous Co₃O₄, MnO₂, NiO, CeO₂, and Fe₂O₃ are prepared by the nanocasting and the supported Pd on mesoporous oxide catalysts are obtained by the chemical reduction method. It is revealed that mesoporous oxides play an important role on Pd dispersion as well as the redox behavior of Pd, which determines the final FAL conversion. Among the catalysts used, Pd/Co₃O₄ shows the highest conversion in FAL hydrogenation and distinct product selectivity toward 2-methylfuran (MF). While FAL is converted via two distinct pathways to produce either furfuryl alcohol (FA) via aldehyde hydrogenation or MF via hydrogenolysis, MF as a secondary product is derived from FA via the hydrogenolysis of C-O over the Pd/Co₃O₄ catalyst. It is revealed that FAL is hydrogenated to FA preferentially on the Pd surface; then the secondary hydrogenolysis to MF from FA is further promoted at the interface between Pd

and Co_3O_4 . We confirm that the reaction pathway over $\text{Pd}/\text{Co}_3\text{O}_4$ is totally different from other catalysts such as Pd/MnO_2 , which produces FA dominantly. The characteristics of the mesoporous oxides influence the Pd-oxide interfaces, which determine the activity and selectivity in FAL hydrogenation.

Keywords: Pd nanoparticle, mesoporous oxide, oxide–metal interface, furfural, hydrogenation.

1. Introduction

Metal-supported oxides are the source of the most important catalysts in the chemical industry [1–8]. The oxide support basically disperses and supports the metal evenly, and also plays a crucial role in influencing the properties of metal. Catalytic properties are greatly affected by oxide supports, which change the dispersion of active metals [9], increase the stability of metals, provide sites to form a new configuration of adsorbed intermediates, and induce charge transfer at created interfaces [10–16]. Many previous studies demonstrated the improvement in activity as well as the change in selectivity of catalytic reaction, owing to the effect of the oxide–metal interface [17–28]. For example, Pt nanoparticle (NP)-loaded mesoporous oxides showed great enhancements of CO oxidation rates depending on the type of oxides (Co_3O_4 , NiO, MnO_2 , Fe_2O_3 , and CeO_2) [12]. The redox behaviors of the oxides resulted in charge transfer at the oxide–metal interface, which amplified the activity of CO oxidation. Kijeński et al. demonstrated not only strong metal–oxide interaction but also strong oxide–oxide interaction, which affected both catalytic activity and selectivity using the Pt deposited on oxides (SiO_2 , $\gamma\text{-Al}_2\text{O}_3$, MgO, TiO_2), which were further covered by the transition metal oxide monolayer (TiO_2 , V_2O_5 , ZrO_2) [29]. Thus, choosing an appropriate oxide support is still considered as an important process not only to develop new catalysts but also to understand thoroughly the catalytic phenomena.

While fossil fuels are still being used as the main energy source and raw material for chemicals in the global market, the development of alternative materials based on biomass has been steadily progressing to solve environmental problems and reduce dependence on petroleum. Among the biomass derivatives, furfural (FAL) has been identified as one of the most promising chemicals for sustainable production of fuels and chemicals [30–41]. However, its undesirable storage properties requires further upgrade to more stable products in order to incorporate them to a petroleum-derived fuel or use them as chemicals. FAL is catalytically converted into furan (FN), 2-methylfuran (MF), and furfuryl alcohol (FA), through one of various chemical reactions, such as decarbonylation, hydrogenolysis, or hydrogenation. FA can be used as a potential fuel/fuel additive or solvent for the production of resins [40].

The selective deoxygenation to MF is of particular interest because this compound has been proposed as a potential additive to gasoline owing to its suitable energy density, boiling point, and octane number, as well as its being a good chemical intermediate [42–47]. The challenge is to find an efficient catalyst, which possesses high activity and controllable selectivity for the production of highly desirable products, while maintaining long-term stability. Many heterogeneous catalysts have been investigated for the hydrogenation of FAL, with the majority of studies focusing on Cu-, Ni- [48], Ru-[49], Pd-[50-52] or PdCu-based[53,54] systems. Among them, Pd is an ideal catalyst for hydrogenation processes, as it readily dissociates hydrogen under ambient conditions. On Pd catalysts, FAL binds strongly through its aromatic ring, resulting primarily in decarbonylation to produce FN. Processes such as aldehyde hydrogenation and hydrodeoxygenation, which are desirable for conversion of aldehydes to fuels such as MF, do not occur readily [51].

In this study, three-dimensional ordered mesoporous oxides of Co_3O_4 , MnO_2 , NiO , CeO_2 , and Fe_2O_3 were synthesized through nanocasting from mesoporous silica (SBA-15) and loaded

with Pd NPs by chemical reduction to investigate the supporting effects on liquid-phase FAL hydrogenation. The properties of Pd-supported mesoporous oxide catalysts such as oxidation states, redox properties, and metal–support interactions are correlated with catalytic activity and selectivity in FAL hydrogenation.

2. Experimental section

2.1. Catalyst preparation

Mesoporous silica SBA-15 with highly ordered hexagonal pore structure was used as a hard template [55, 56]. For the preparation of SBA-15, 16 g of pluronic P123 was dissolved in 120 g of water and 480 g of 2 M HCl solution at 40 °C. Then 34 g of TEOS was added into that solution with stirring at 40 °C for 20 h. The mixture was aged at 80 °C overnight without stirring. The solid product was recovered, washed, and air-dried at room temperature. Calcination was carried out by slowly increasing the temperature from room temperature to 550 °C for 8 h and maintaining at 550 °C for 6 h.

The nanocasting approach using SBA-15, which was developed by Schüth and co-workers [51, 55], was used to prepare mesoporous oxides. $\text{Co}(\text{NO}_3)_2 \cdot 6\text{H}_2\text{O}$, $\text{Ni}(\text{NO}_3)_2 \cdot 6\text{H}_2\text{O}$, $\text{Mn}(\text{NO}_3)_2 \cdot x\text{H}_2\text{O}$, $\text{Ce}(\text{NO}_3)_3 \cdot 6\text{H}_2\text{O}$, and $\text{Fe}(\text{NO}_3)_3 \cdot 9\text{H}_2\text{O}$ (Sigma-Aldrich) were used without further purification to synthesize mesoporous Co_3O_4 , NiO, MnO_2 , CeO_2 , and Fe_2O_3 , respectively [12, 57–59]. In a typical synthesis, 24 mmol of metal nitrate was dissolved in 6 mL of water. Then, the solution was added to 6 g of SBA-15 in 30 mL of toluene at 65 °C with stirring. After evaporation of toluene, the resulting sol was collected and dried at 60 °C overnight, followed by calcination at 300 °C for 5 h. The silica templates were removed completely using 2 M aqueous NaOH solution heated to 90 °C followed by washing steps with water and a final drying step at 50 °C.

The oxide-supported Pd catalysts were prepared by the chemical reduction method as follows [13]: A predetermined amount of H_2PdCl_4 solution was added dropwise to a solution of trisodium citrate ($\text{Na}_3\text{C}_6\text{H}_5\text{O}_7$, 0.526 mM, Pd/trisodium citrate ratio = 10:1, Sigma-Aldrich, > 98%), which was maintained at 5 °C under stirring. The sodium hydroxide (NaOH, 0.2 M aqueous solution, Sigma-Aldrich, > 98%) was then added to adjust the pH of the resulting solution to ~7. The obtained mesoporous oxides were combined with the Pd solution to give 5 wt.% of Pd. Thereafter, an ice-cold sodium borohydride solution (5 mL of a 0.3 M NaBH_4 solution, Sigma-Aldrich, 98%) was added slowly, and maintained by stirring for 3 h at 5 °C. The catalysts were collected by filtration and washed with deionized water repeatedly until the pH of the filtrate was 6. The final catalysts were retrieved and dried at 105 °C for 5 h.

2.2. Catalyst characterization

Various techniques were used for the characterization of Pd NP supported on mesoporous oxide catalysts. A structure of catalysts was characterized by transmission electron microscopy (TEM, JEOL JEM-1400) and high-resolution TEM (HRTEM, JEOL JEM-2100F). Surface textural parameters were measured by nitrogen adsorption using a BESORP-max unit. An inductively coupled plasma optical emission spectrometry (ICP-OES, Varian 700-ES) was used for the quantification of Pd loading. X-ray diffraction (XRD) patterns were collected on a PANalytical X'Pert PRO diffractometer using a Cu $\text{K}\alpha$ radiation source ($\lambda = 0.154056$ nm). The Pd dispersion was measured by the CO adsorption capacity using CO chemisorption instrument (Auto Chem II 2920, and Micromeritics Instruments Co., USA). Diffuse reflectance infrared Fourier transform (DRIFT) spectroscopy by CO adsorption was carried out over Pd-supported oxide catalysts using a spectrometer (Nicolet iS10 FTIR) equipped with a DRIFT cell and mercury-cadmium-telluride detector. Samples were diluted with KBr and loaded into a DRIFT cell (Harrick Scientific) with ZnSe windows. All IR spectra were collected for 128 scans with

4 cm⁻¹ resolution. Samples were pretreated at 150 °C for 1 h under He (flow rate = 1 mL/s). CO adsorption was performed using 0.2% CO/He (flow rate = 1 mL/s) at room temperature. The collected spectrum was normalized by the number of CO adsorbed on Pd sites from CO chemisorption, which was obtained separately.

2.3. Catalytic FAL hydrogenation

A supported Pd catalyst (10 mg) was mixed with FAL (1 g, Acros, 99%) and isopropanol (20 mL, Sigma-Aldrich) in a 100 mL stainless-steel autoclave reactor (Parr 5500) [13]. After the reactor was sealed, air was purged by flushing four times with hydrogen and then pressurized with hydrogen to 20 bar. If not enough hydrogen was provided, FAL conversion was very low (Fig. S1). The solution containing the supported Pd catalyst was stirred under 600 rpm at 180 °C for 5 h. After completion of the reaction, the catalyst particles were removed from the solution, and the product analysis was conducted by gas chromatography using a flame ionization detector (FID; Agilent 7820A) equipped with a capillary column (DB-Wax, 30 m length, 0.32 mm internal diameter, 0.25 µm film thickness). As a substrate chemical, FA (Sigma-Aldrich, 98%), THFA (Sigma-Aldrich, 99%), FN (Sigma-Aldrich, 99%), THF (Alfa Aesar, 99%), and MF (Sigma-Aldrich, 99%) were tested for the identification of products. The product conversion and selectivity were determined as follows:

$$\text{Conversion (\%)} = \frac{\text{mol furfural consumed}}{\text{mol furfural fed}} \times 100$$

$$\text{Selectivity (\%)} = \frac{\text{mol product formed}}{\text{mol furfural consumed}} \times 100$$

3. Results and discussion

3.1. Characterization of catalysts

Highly dispersed Pd catalysts supported on various mesoporous oxides were prepared by chemical reduction using sodium borohydride, in the presence of trisodium citrate as a stabilizer [13]. The Pd content in Pd/oxide catalysts was determined by ICP-OES as presented in Table 1. The results confirmed that approximately 5 wt.% of Pd was presented in all samples. The Pd dispersions of the various catalysts were calculated based on CO adsorption measurements (Table 1), with a dispersion of 29.3% and 28.9% being achieved for the Pd/Co₃O₄ and Pd/MnO₂ catalysts, respectively, which were significantly greater than those of Pd-supported NiO, CeO₂ and Fe₂O₃. N₂ adsorption–desorption isotherms of the Pd/oxides show type IV isotherms with a clear hysteresis loop at 0.4–0.9 of the relative pressure (p/p_0) (Fig. S2), revealing the presence of uniform mesopores. The texture parameters of Pd/oxide catalysts are summarized in Table 1. All Pd/oxide catalysts show high surface areas (82–172 m²·g⁻¹), in which Pd/Co₃O₄ (172 m²·g⁻¹) exhibits the highest surface area.

Table 1. Characterization of Pd/oxide catalysts.

Catalyst	Pd loading (wt.%)		CO-TPD Pd dispersion (%)	Surface area (m ² ·g ⁻¹)	BET		Chemisorbed CO (mol·g ⁻¹) ^b		
	Nominal	Actual ^a			Pore volume (cm ³ ·g ⁻¹)	Nominal	Actual ^a	Pd dispersion (%)	Surface area (m ² ·g ⁻¹)
Pd/Co ₃ O ₄	5.0	5.8	29.3	172	0.33	7.8	2.91	13.00	0.22
Pd/MnO ₂	5.0	7.4	28.9	131	0.50	15.1	6.80	13.20	0.51
Pd/NiO	5.0	6.2	18.9	85	0.27	12.6	1.79	9.14	0.20
Pd/CeO ₂	5.0	7.7	13.0	82	0.32	15.7	2.93	6.43	0.45
Pd/Fe ₂ O ₃	5.0	5.8	2.6	139	0.40	11.4	-	-	-

^a Measured from ICP-AES

^b Measured from CO-TPD and DRIFT spectroscopy (CO adsorption)

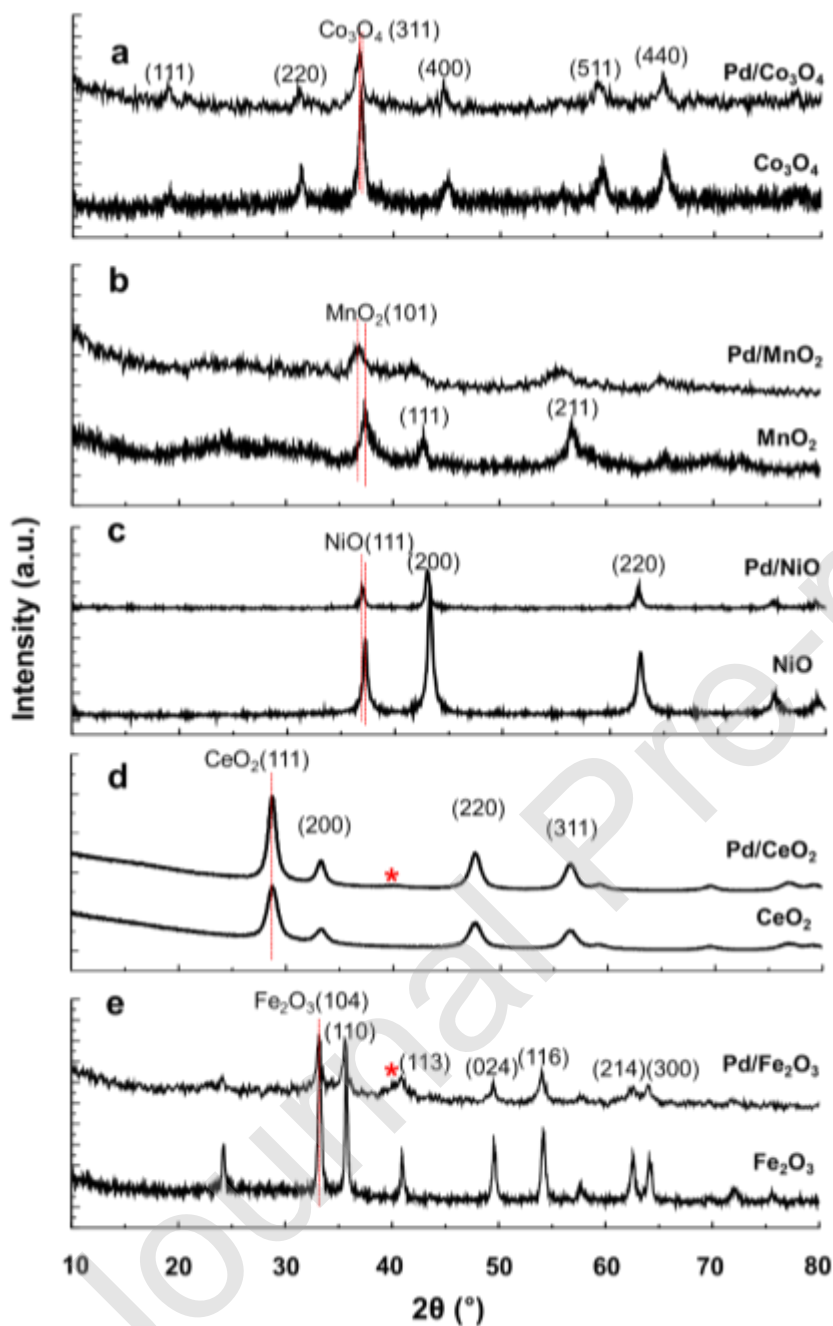


Fig. 1. XRD patterns of (a) Pd/Co₃O₄ and Co₃O₄, (b) Pd/MnO₂ and MnO₂, (c) Pd/NiO and NiO, (d) Pd/CeO₂ and CeO₂, and (e) Pd/Fe₂O₃ and Fe₂O₃. The peaks corresponding to the oxides are indexed.

Crystallographic information about the prepared oxide and Pd/oxide catalysts is obtained from XRD measurements as shown in Fig. 1. XRD patterns of the resulting mesoporous oxides are well-matched to Co_3O_4 (JCPDS 42-1467), MnO_2 (JCPDS 04-779), NiO (JCPDS 47-1049), CeO_2 (JCPDS 43-1002), and Fe_2O_3 (JCPDS 33-0664). The broadening and well-resolved diffraction peaks are attributed to the high crystallinity of the mesoporous oxides. No diffraction peaks of Pd species, including Pd^0 or PdO , are observed on the $\text{Pd}/\text{Co}_3\text{O}_4$, Pd/MnO_2 , and Pd/NiO catalysts, indicating that the Pd species are highly dispersed on the catalyst surface or Pd atoms and/or ions are incorporated into the crystal lattice of oxides. The peaks corresponding to oxides are shifted in the negative direction after introducing Pd into oxides except Fe_2O_3 and CeO_2 , probably due to a crystal lattice distortion. For the $\text{Pd}/\text{Fe}_2\text{O}_3$ and Pd/CeO_2 catalysts, a small peak at 40° is observed, which is associated with Pd^0 (JCPDS 65-2867), suggesting that Pd was segregated and not incorporated into the Fe_2O_3 and CeO_2 structure evenly.

Fig. 2 shows the TEM images of Pd/oxide catalysts. Apparently, all oxides prepared by the nanocasting method display a well-ordered mesoporous structure. Almost all the obtained catalysts have rod-like morphology, which is replicated from the SBA-15 template, indicating good replication of the silica template. The Pd NPs with sizes smaller than 5 nm were highly dispersed on the surface of mesoporous MnO_2 and NiO , while there are some aggregations of Pd particles on mesoporous CeO_2 and Fe_2O_3 . This observation is consistent with the CO-TPD and XRD results.

Fig. 3 shows the bright-field scanning transmission electron microscopy (BF-STEM), high angle annular dark-field scanning transmission electron microscopy (HAADF-STEM) and energy dispersive spectroscopy (EDS) mapping images of $\text{Pd}/\text{Co}_3\text{O}_4$ and $\text{Pd}/\text{Fe}_2\text{O}_3$ catalysts. Apparently, the mesoporous Co_3O_4 displayed a well-defined ordered mesoporous structure, and the loading of Pd did not alter the mesoporous architecture (Figs. 3a–b). As shown in the high-resolution BF-STEM images of the $\text{Pd}/\text{Co}_3\text{O}_4$ catalysts (Fig. 3b), the intraplanar spacings (d values) were measured

to be approximately 0.47 and 0.22 nm, which closely agree with that of the (111) crystal plane of the standard Co_3O_4 (JCPDS 42-1467) and that of the (111) crystal plane of the standard Pd (JCPDS 65-2867), respectively. The HAADF-STEM and EDS mapping images (Figs. 3c–f) show a highly dispersed Pd NPs on the surface of the mesoporous Co_3O_4 . In contrast, the Pd NPs of the Pd/ Fe_2O_3 catalysts (Figs. 3g–l) form large aggregates with diameters larger than 6 nm.

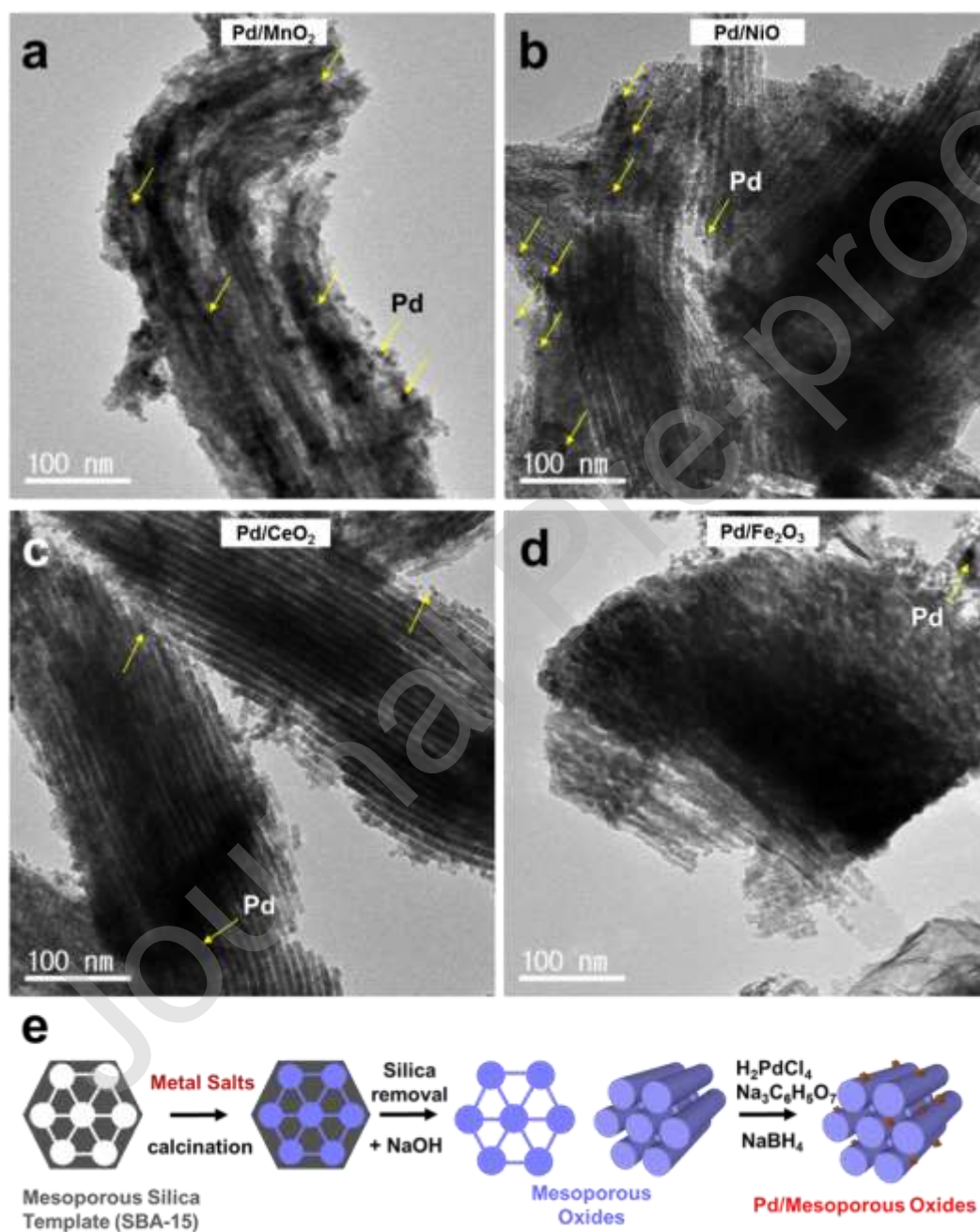


Fig. 2. TEM images of (a) Pd/MnO₂, (b) Pd/NiO, (c) Pd/CeO₂, and (d) Pd/Fe₂O₃. (e) Illustration of the nanocasting approach for the preparation of Pd/oxide catalysts.

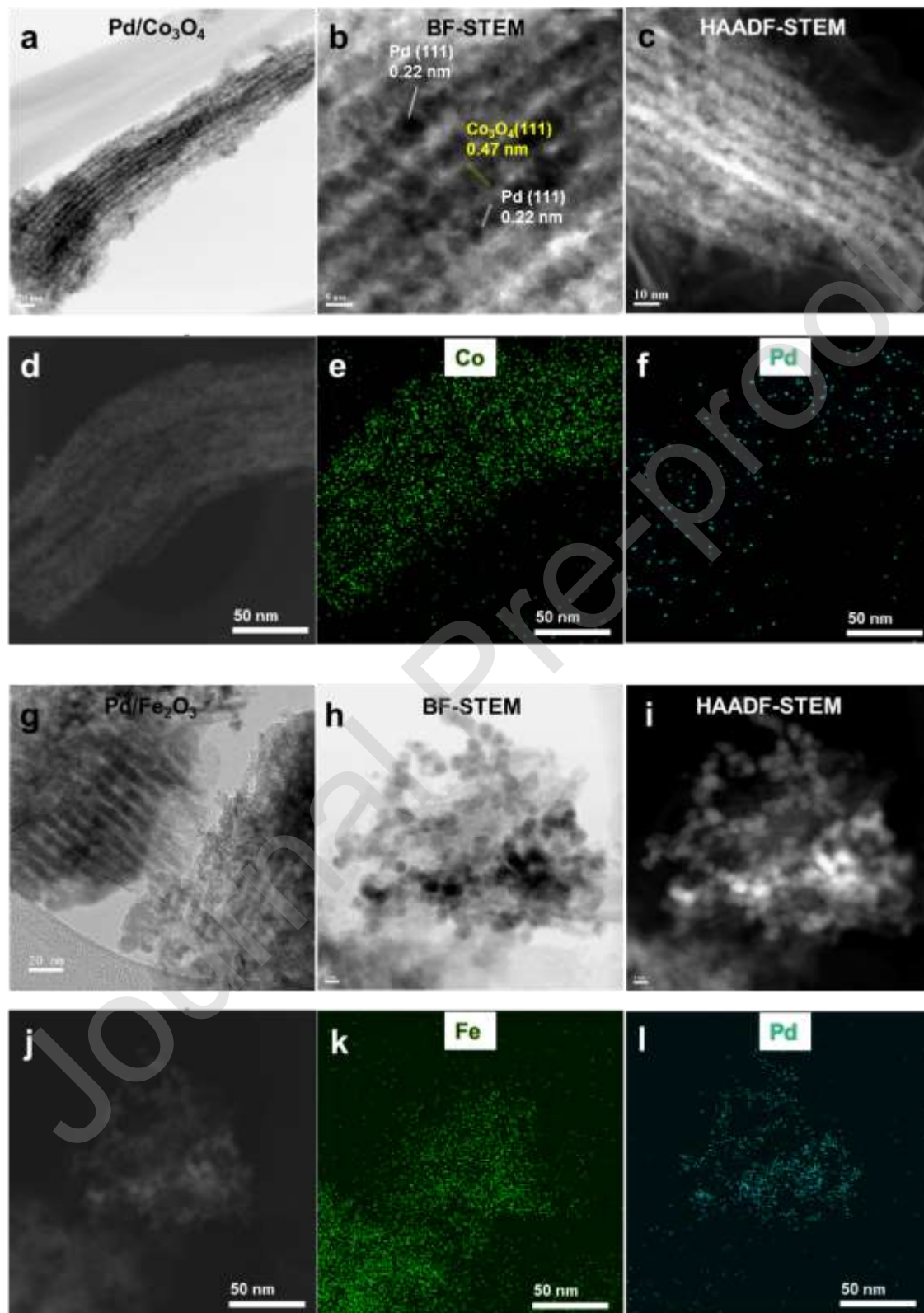


Fig. 3. HR-TEM, BF-STEM, HAADF-STEM, and EDS mapping of (a–f) Pd/Co₃O₄, and (g–l) Pd/Fe₂O₃ catalysts.

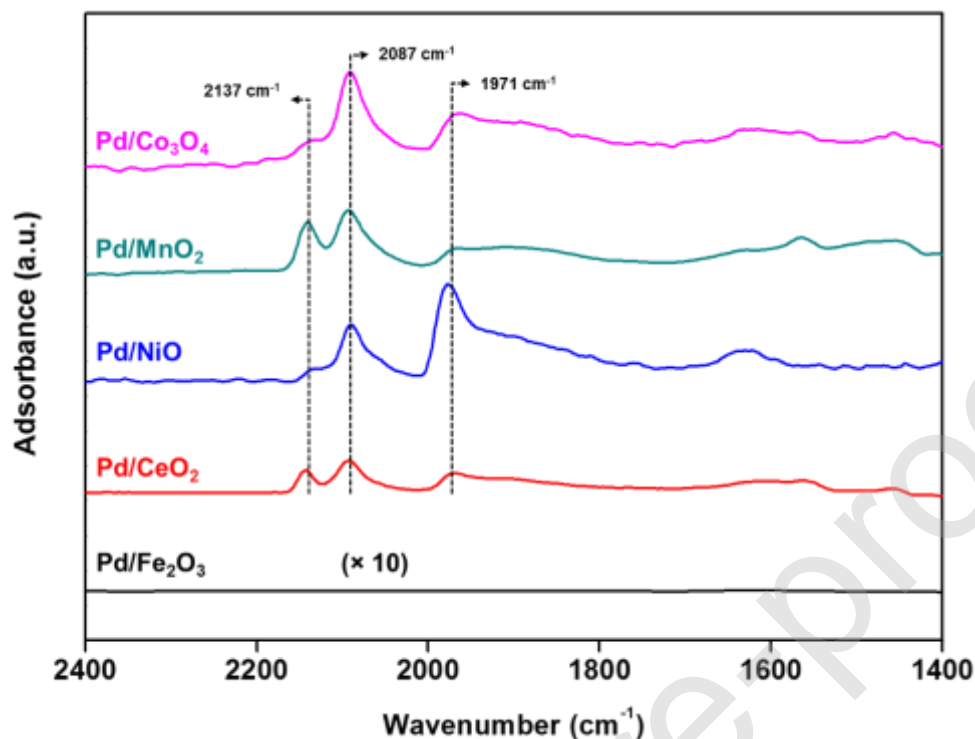


Fig. 4. DRIFT spectroscopy results by CO adsorption on Pd/oxide catalysts.

DRIFT spectroscopy after adsorption of CO as a probe molecule provides valuable information about oxidation states and characteristic metal sites [60–62]. Fig. 4 shows the CO adsorbed DRIFT absorption spectra of various Pd/oxide catalysts at room temperature. The bands at 1800–2300 cm⁻¹ are associated with the adsorbed CO on metal surfaces. Pd/Co₃O₄, Pd/MnO₂, Pd/NiO, and Pd/CeO₂ show two bands at 1971 cm⁻¹ and 2087 cm⁻¹ after CO adsorption which are assigned to metallic Pd⁰ as a bridge mode and linear CO adsorbed Pd⁰ sites, respectively. The peak at 2137 cm⁻¹ is ascribed to CO adsorbed on Pd²⁺ sites [61, 62]. The relative molar ratios of PdO/Pd⁰ calculated by DRIFT spectra (see Fig. S3) are summarized in Table 1. Interestingly, no adsorption bands appeared on the Pd/Fe₂O₃ catalyst (Fig. 4). We further conduct DRIFT experiments on Pd/Fe₂O₃ at different conditions: thermal treatment under He (60 sccm) at 120 °C for 1 h, and oxidation under 20%

O₂/He (60 sccm) at 250 °C for 1 h. As shown in Fig. S4a, there are no peaks corresponding to Pd²⁺ and Pd⁰ on the Pd/Fe₂O₃ under He treatment, while the peak at 2137 cm⁻¹ assigned to CO adsorbed on Pd²⁺ sites, appears on Pd/Fe₂O₃ after oxidation treatment. The full range DRIFT spectra of CO adsorbed on Pd/oxide catalysts under He treatment (Fig. S4b) show that two bands at 2839 – 2972 cm⁻¹ and 1578 – 1718 cm⁻¹, which are assigned to C–H bending and C=O stretching, respectively, appear only on the Pd/Fe₂O₃. After oxidation at 250 °C using 20% of O₂/He, these bands disappeared (Fig. S4c). We speculate that the main reason for the absence of CO adsorption on Pd/Fe₂O₃ in DRIFT spectra is due to the surfactant (trisodium citrate) which covers the Pd surface of the Pd/Fe₂O₃ catalyst [63]. For the other Pd/oxide catalysts, there is no band corresponding to C–H bending and C=O stretching, indicating that surfactants are completely removed through the washing and drying steps.

3.2. Catalytic activity

The hydrogenation of FAL is carried out over the oxide-supported Pd catalysts (5 wt.%) and the mesoporous oxides to examine the effect of metal dispersion and type of support on catalytic activity and selectivity. As shown in Fig. 5, all as-synthesized mesoporous oxides without Pd loading show a very low activity in FAL conversion. For instance, approximately 3% of FAL conversion was obtained with MnO₂, NiO, CeO₂, and Fe₂O₃ and 13% of FAL conversion with Co₃O₄. When Pd NPs were loaded into the mesoporous oxides via the chemical reduction, the catalytic activity observed was significantly higher than that of mesoporous oxide without Pd loading. It is clearly observed that the catalytic activity of oxide-supported Pd catalysts on FAL hydrogenation decreased in the order of Pd/Co₃O₄ (100%) > Pd/MnO₂ (83%) > Pd/NiO (68 %) > Pd/CeO₂ (22%) > Pd/Fe₂O₃ (18%). This catalytic behavior is attributed to two possibilities: first, activity from Pd active sites on the support surface and second, activity at the oxide–metal interface [12]. In Table 1, the Pd dispersion is decreased

similarly in the following order: Pd/Co₃O₄ (29.3%) > Pd/MnO₂ (28.9%) > Pd/NiO (18.9%) > Pd/CeO₂ (13%) > Pd/Fe₂O₃ (2.6%). This indicates that a high Pd dispersion induces high conversion in FAL hydrogenation reaction. Pd/Co₃O₄, Pd/MnO₂, and Pd/NiO with high Pd dispersion exhibit much higher conversions than Pd/CeO₂ and Pd/Fe₂O₃. Surprisingly, Pd/CeO₂ exhibits a catalytic performance similar to Pd/Fe₂O₃, even though it showed a higher Pd dispersion than Pd/Fe₂O₃.

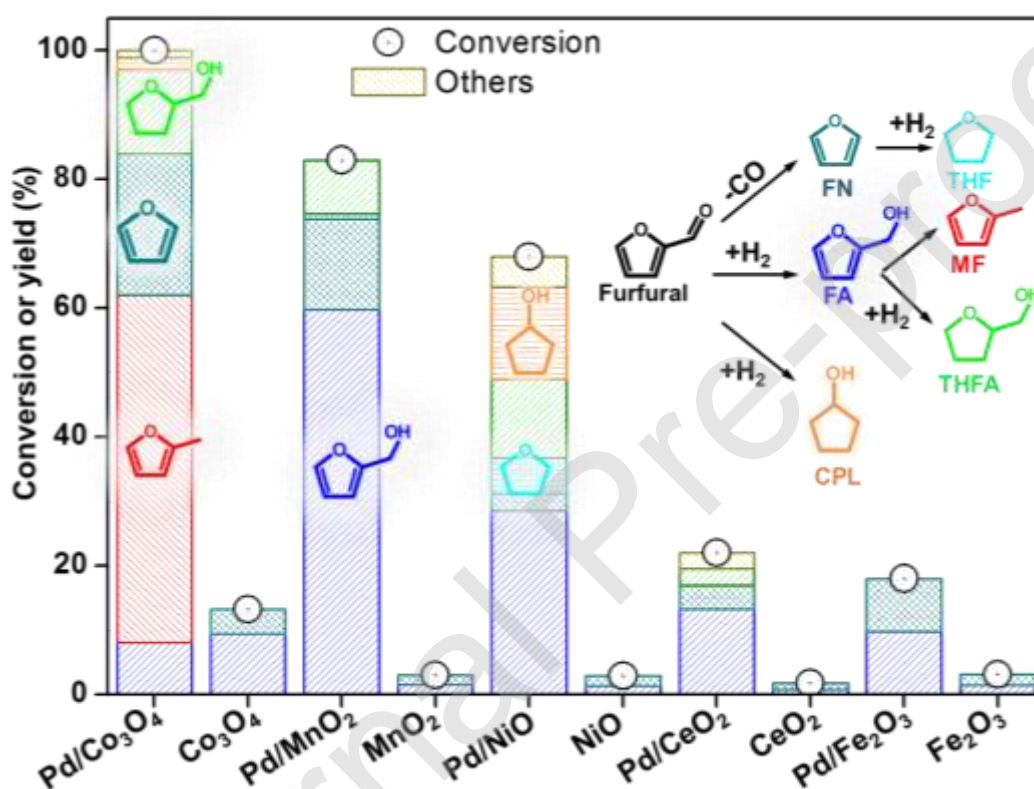


Fig. 5. Product distribution from FAL conversion over various catalysts. Reaction conditions: FAL = 1 g, isopropanol = 20 mL, catalyst = 10 mg, H₂ = 20 bar, reaction temperature = 180 °C, reaction time = 5 h, and stirring speed = 600 rpm.

We also compared FAL conversion over the prepared by the catalysts which prepared by the typical impregnation method (Table S1). While overall FAL conversion of the Pd/oxide prepared by the impregnation were much less than those of Pd/oxides prepared by the chemical

reduction, the impregnated Pd/NiO catalyst exhibited the best FAL conversion (50 %) (Fig. S5). In our previous report, chemical reduction by sodium borohydride has already proven to be effective for the preparation of highly dispersed and ultrafine Pd catalyst on various oxides, compared to conventional impregnated Pd/oxide catalysts. When the mesoporous oxide supports were replaced with a commercially available oxide support, the FAL conversion was significantly reduced. For example, when preparing Pd/Co₃O₄ and Pd/MnO₂ catalysts composed of commercial Co₃O₄ (Sigma-Aldrich, powder <10 μm) and MnO₂ (Sigma-Aldrich, powder <10 μm), the FAL conversions were 80 and 16 %, respectively, due to the low surface area and poor Pd dispersion. From these results, it was revealed that Pd/oxides catalysts prepared by the chemical reduction were highly active catalysts for FAL hydrogenation as compared to the impregnated Pd/oxide catalysts. The mesoporous oxides further improved Pd dispersion than commercial oxides with low surface area. In our previous study, mesoporous carbons, including CMK-3, CMK-5, CMK-8, and MSU-F-C, were used as carbon supports to produce Pd/C catalysts to investigate the effect of pore size and structure of carbons [64]. It was revealed that CMK-5 with the largest surface area and hexagonal hollow tubular framework was the most efficient carbon support for Pd/C catalysts, with the highest conversion of FAL in isopropanol. The FAL conversion was greatly influenced by the surface area of carbons and the corresponding Pd dispersion. It is demonstrated that the activity in FAL hydrogenation was determined by the surface area of carbons. In the present study, the effect of mesopores is not prevalent, because the average size and structure of mesoporous Co₃O₄, MnO₂, NiO, CeO₂, and Fe₂O₃ are the same.

Depending on the type of mesoporous oxide, the Pd dispersion was varied due to the specific interfacial effect. The DRIFT spectroscopy results during CO adsorption on Pd/oxide catalysts prepared by the chemical reduction after H₂ reduction under reaction conditions (180 °C)

provide the degree of reduction of surface Pd (Fig. S6). Interestingly, Pd/CeO₂ exhibited a lower Pd reducibility than other catalysts. After 1 h pretreatment under a flow of 10% H₂/He at 180 °C, Pd/Co₃O₄, Pd/MnO₂ and Pd/NiO were totally reduced, while there is a peak corresponding to PdO on Pd/CeO₂. The intensity of Pd⁰ peak was decreased over Pd/Co₃O₄, Pd/MnO₂, and Pd/NiO catalysts after reduction, indicating that there was a strong interfacial effect between Pd and oxides (Co₃O₄, MnO₂, and NiO). Therefore, we speculate that the Pd species were fully reduced under the reaction condition except for the Pd/CeO₂ catalyst, which induces a low catalytic activity of Pd/CeO₂. In catalytic selectivity, the main product obtained by the FAL hydrogenation over the Pd/MnO₂, Pd/NiO, Pd/CeO₂, and Pd/Fe₂O₃ catalysts was FA, while MF was the dominant product over the Pd/Co₃O₄ catalyst. Although Pd/MnO₂ and Pd/Co₃O₄ have the same Pd dispersion (approximately 29%), Pd/Co₃O₄ exhibits a much higher FAL conversion with preferred selectivity toward MF. While the mesoporous Co₃O₄ without Pd shows low activity, it is revealed that not only the Pd active site but also the oxide–metal interface contribute to the activity of Pd/Co₃O₄. As such, the binding energy (BE) shift in XPS spectra of Co₃O₄ surface before and after Pd loading (Fig. S7) demonstrates the creation of a new interface between Pd and Co₃O₄. The Co 2p_{3/2} signal at BE = 779.4 eV indicates the presence of surface Co³⁺, whereas the Co 2p_{3/2} signal at BE = 780.9 eV refers to the surface Co²⁺. It is observed that after deposition of Pd NPs on a mesoporous Co₃O₄, the surface Co²⁺/Co³⁺ molar ratio increases from 0.76 to 2.16, indicating that the surface Co²⁺ concentration increases significantly via the reaction of Pd⁰ + Co³⁺ → Pd²⁺ + Co²⁺. The change in oxidation state of Co₃O₄ is due to charge transfer from Pd NPs to Co₃O₄, in which the oxidized Pd²⁺ species in the Pd/Co₃O₄ further promotes high distribution of Pd on Co₃O₄ (Fig. S8). The existence of oxidized Pd²⁺ species (Fig. S9) and the BE shift in XPS spectra of oxides surface before and after Pd addition on Pd/MnO₂, Pd/NiO, Pd/CeO₂, and Pd/Fe₂O₃ catalysts (Fig. S10) indicate that new interfaces are generated between Pd and the oxide.

Although the original surface area of mesoporous oxides determines the Pd dispersion of the supported catalysts (Table 1), the relative ratio of Pd⁰ to PdO in the Pd/oxide catalysts further influences the overall catalytic behaviors.

In order to confirm the reaction behaviors on Pd/oxide catalysts, FAL hydrogenation was conducted at different reaction times. Fig. 6a illustrates the FAL conversion as a function of reaction time over Pd/oxide catalysts at 180 °C. Based on the data shown in Fig. 6a, the FAL hydrogenation activities have the following order: Pd/Co₃O₄ > Pd/MnO₂ > Pd/NiO > Pd/CeO₂ > Pd/Fe₂O₃. The first-order dependence of FAL hydrogenation reaction using Pd/oxide catalysts were supported by the linearity of -ln(1 - X) versus time plots in Fig. 6b, where X is the FAL conversion. As the first-order dependence of the reaction was validated, the apparent reaction rate constants of FAL hydrogenation (k_{app}) were determined from the slope of the plot of $-\ln(1 - X) = k_{app} \times t$ and summarized in Table 2. The apparent rate constant of Pd/Co₃O₄ was much greater than those of other catalysts. The k_{app} values were 13×10^{-3} , 5.6×10^{-3} , 2.4×10^{-3} , 1.1×10^{-3} , and $0.9 \times 10^{-3} \text{ min}^{-1}$ for Pd/Co₃O₄, Pd/MnO₂, Pd/NiO, Pd/CeO₂, and Pd/Fe₂O₃, respectively. The results also confirmed that Pd/Co₃O₄ possessed a much higher activity in FAL hydrogenation, compared to Pd/MnO₂, Pd/NiO, Pd/CeO₂, and Pd/Fe₂O₃ catalysts.

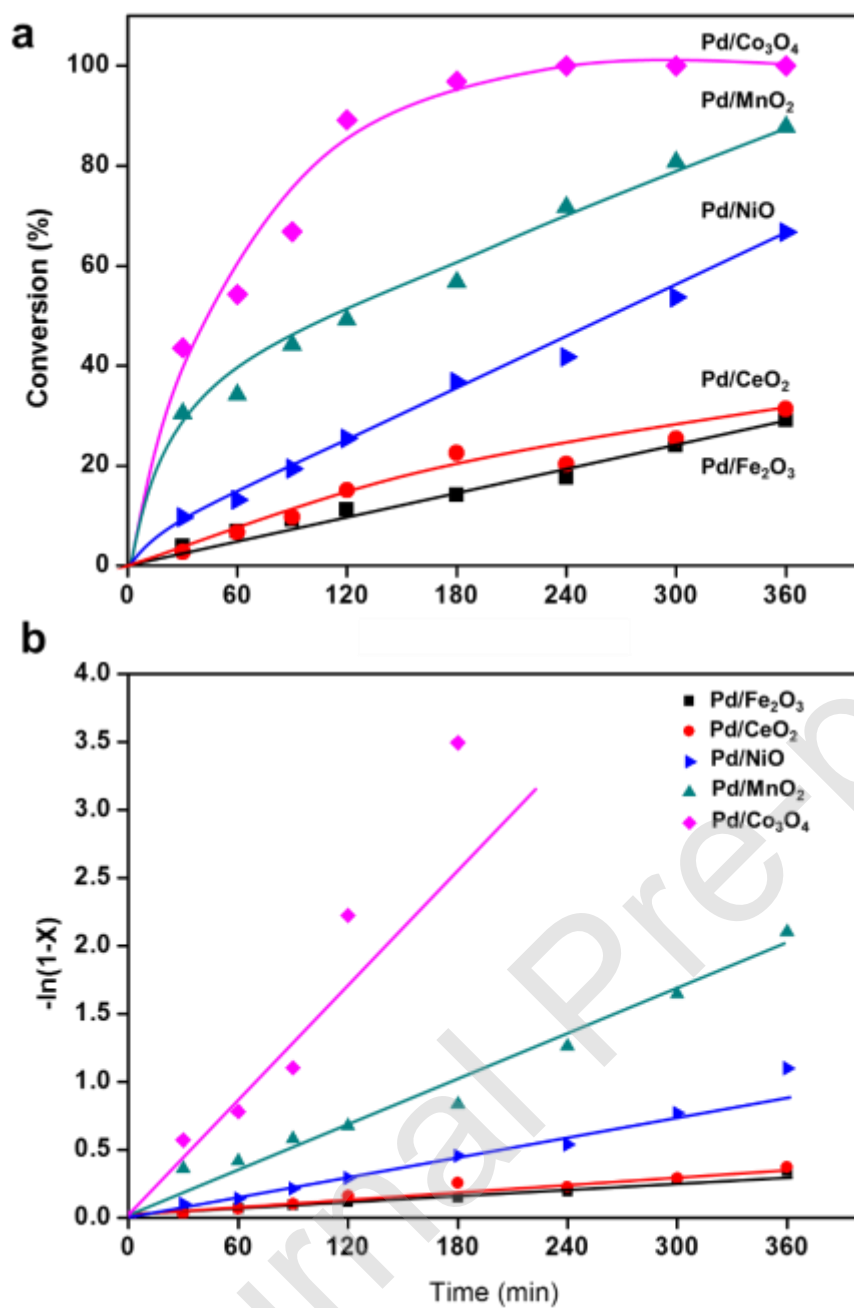


Fig. 6. (a) FAL conversion as a function of reaction time over various supported Pd catalysts. (b) Time dependent FAL conversion. Reaction conditions: FAL = 1 g, isopropanol = 20 mL, catalyst = 10 mg, H₂ = 20 bar, reaction temperature = 180 °C, reaction time = 0.1–5 h, and stirring speed = 600 rpm.

Table 2. Hydrogenation of FAL over mesoporous oxides and Pd/oxides^a

Catalysts	Conversion (%)	k_{app} (min^{-1}) ($\times 10^{-3}$) ^b	Yield (%)						
			FA	MF	FN	THF	THFA	Cyclohexanol	Others
Co ₃ O ₄	13	-	9.44	-	3.73	-	-	-	-
MnO ₂	3	-	1.52	-	1.49	-	-	-	-
NiO	3	-	1.34	-	1.61	-	-	-	-
CeO ₂	2	-	0.81	-	0.94	-	-	-	-
Fe ₂ O ₃	3	-	1.40	-	1.73	-	-	-	-
Pd/Co ₃ O ₄	100	13	8.00	54	22	-	13	2	1
Pd/MnO ₂	83	5.6	59.76	-	14.11	0.83	8.3	-	-
Pd/NiO	68	2.4	28.56	-	2.72	5.44	12.24	14.28	4.76
Pd/CeO ₂	22	1.1	13.20	-	3.74	-	2.64	-	2.42
Pd/Fe ₂ O ₃	18	0.9	9.72	-	8.28	-	-	-	-
Pd/SiO ₂	6	-	3.72	-	1.04	0.51	0.49	0.45	-

^a Reaction conditions: FAL = 1 g, isopropanol = 20 mL, catalyst = 10 mg, H₂ = 20 bar, reaction temperature = 180 °C, reaction time = 5 h, stirring speed = 600 rpm.

^b Apparent first-order reaction rate constant evaluated from the slope of the plot of $\ln(1 - X) = -k_{app} \times t$.

To investigate the reaction pathways, Pd/Co₃O₄ and Pd/MnO₂, which have totally different selectivity results were selected and compared for the FAL hydrogenation. The FAL conversion and product selectivity as a function of reaction time are shown in Fig. 7. As the reaction proceeded, 55% of FAL was converted along with 40 % of FA selectivity after 1 h reaction over the Pd/Co₃O₄ catalyst (Fig. 7a). FA reached a maximum yield of 50% at 2 h and then decreased gradually afterward. The MF yield was very small at the initial time and rapidly increased following the decrease in FA yield. After 10 h, the MF reached a maximum yield of 50%, while the fraction of FA was very low. The yields of FN and THFA were increased over

the entire reaction time until they reached 22% and 10% yield, respectively. From these results, it was proven that FAL was converted quickly to FA as a main intermediate with a maximum selectivity at 2 h, and then MF was produced via hydrogenolysis at the expense of FA after 2 h. In contrast, Pd/MnO₂ had a significant different selectivity behavior from the Pd/Co₃O₄ catalyst (Fig. 7b). It was observed that on Pd/MnO₂ catalyst, FA was produced as a major product from FAL with a small portion of FN and THFA, while MF was hardly obtained. The yield of FA was increased over the entire reaction time until it reached 60 % yield over Pd/MnO₂. These results demonstrate that the FAL hydrogenation over Pd/Co₃O₄ catalyst occurred by the following pathway: aldehyde hydrogenation toward FA and secondary hydrogenolysis to MF. Meanwhile, Pd/MnO₂ promoted only the aldehyde hydrogenation toward FA. To further confirm the reaction pathways over Pd/Co₃O₄ and Pd/MnO₂ catalysts, the hydrogenation of FA was conducted in the same reaction conditions as the FAL hydrogenation. Fig. 8 shows the degradation of FA and product distribution over Pd/Co₃O₄ and Pd/MnO₂ catalysts. Fig. 8a clearly shows that the Pd/Co₃O₄ catalyst converted all of the FA within 3 h, while approximately 5% of FA was degraded simultaneously in the presence of Pd/MnO₂ afterward. It indicates that Pd/MnO₂ exhibits no activity for the reaction of FA. Fig. 8b shows the evolution of product distribution as a function of time over Pd/Co₃O₄ catalyst in the FA hydrogenation. It confirms that on the Pd/Co₃O₄ catalyst, the yields toward MF, FN, and THFA were increased over the entire reaction until it reached 45, 30, and 15%, respectively. In the previous study, Pd/C, Pd/SiO₂, and Pd/Al₂O₃ catalysts were used to investigate the contribution of Pd to catalytic activity and selectivity, while carbon, SiO₂, and Al₂O₃ are known as chemically inert supports [13]. Depending on the type of support, the Pd dispersion changed and the resulting FAL conversion also changed. While Pd/C catalyst showed higher FAL conversion than Pd/SiO₂ and Pd/Al₂O₃, the FAL conversion and THFA selectivity increased with smaller Pd size or Pd dispersion, reaction temperature and time

increased [13]. From these results, it was confirmed that Pd catalyzed FAL hydrogenation is advantageous for producing THFA. However, current research shows that the activity and selectivity changes in various mesoporous oxides supported Pd catalysts due to the specific interfacial effect. For example, the main products of Pd/Co₃O₄ and Pd/MnO₂ are MF and FA, respectively.

Journal Pre-proof

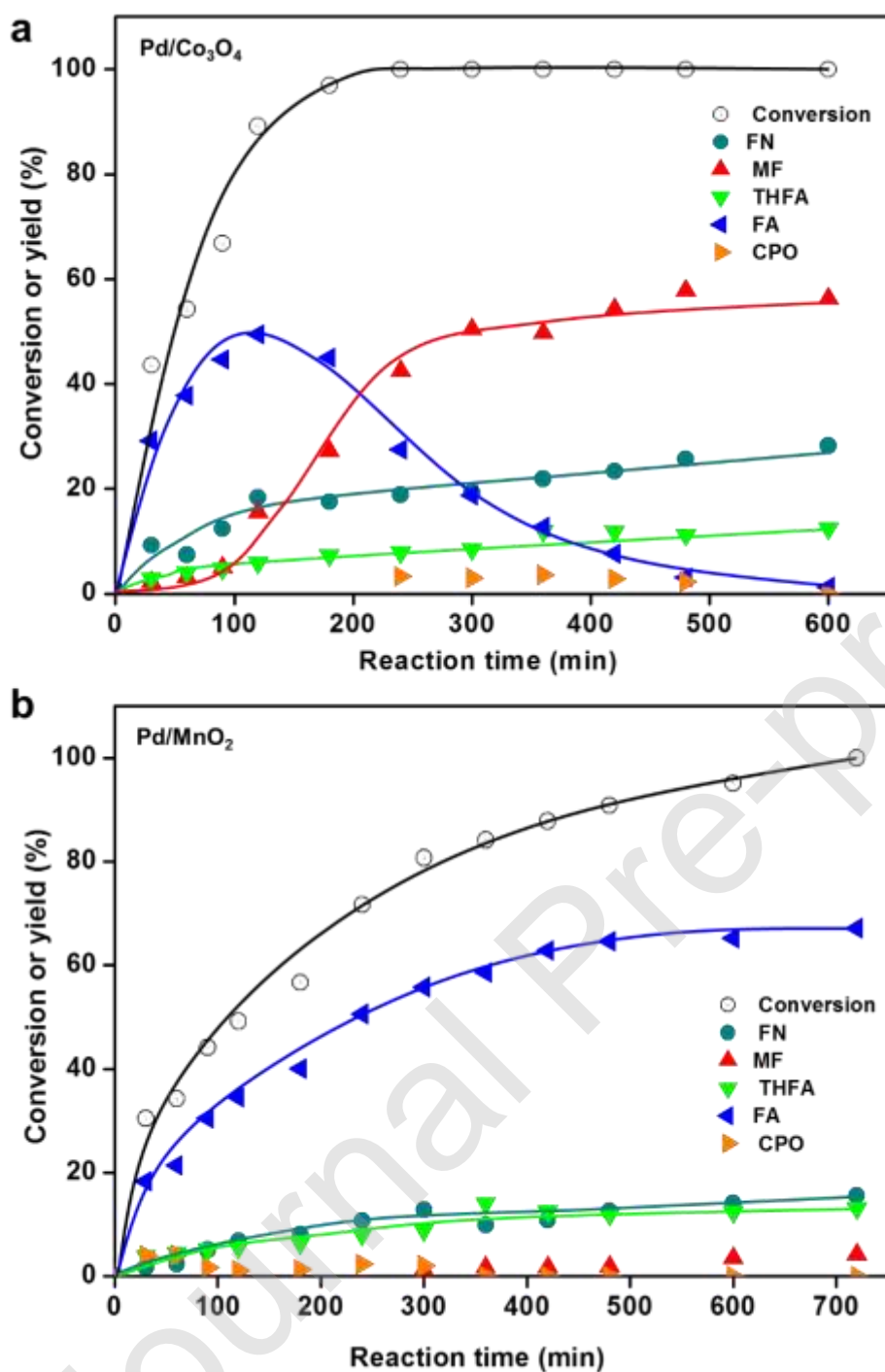


Fig. 7. Effect of reaction time on selectivity and FAL conversion over (a) Pd/Co₃O₄ and (b) Pd/MnO₂ catalyst. Reaction conditions: FAL = 1 g, isopropanol = 20 mL, catalyst = 10 mg, H₂ = 20 bar, reaction temperature = 180 °C, and stirring speed = 600 rpm.

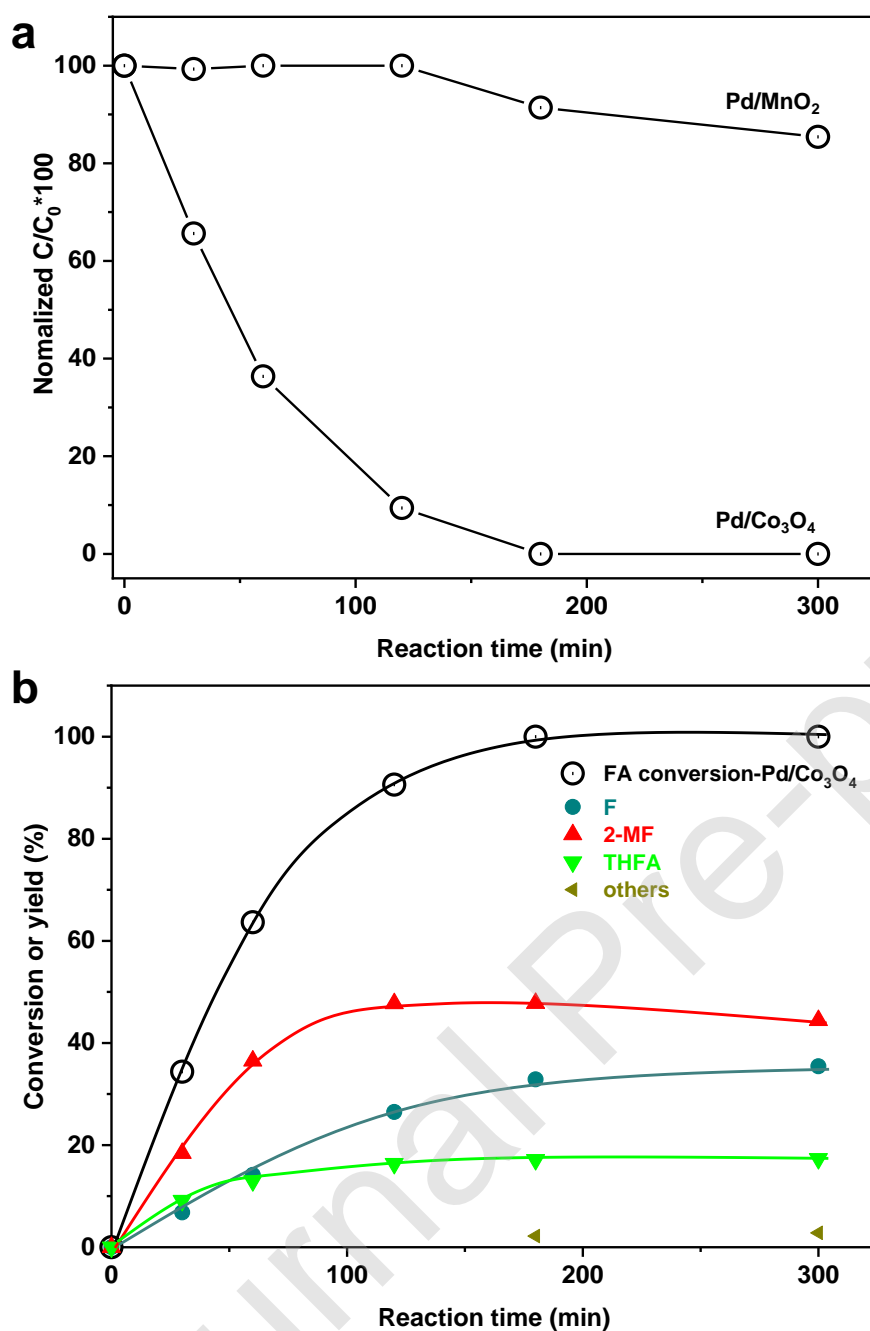
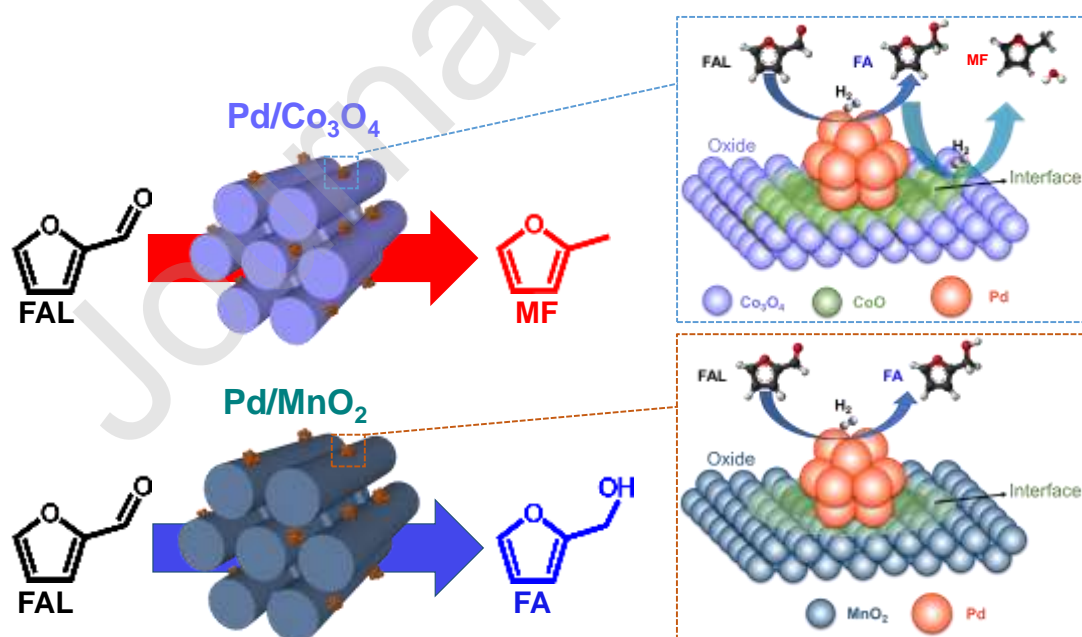


Fig. 8. (a) Change in concentration of FA on Pd/Co₃O₄ and Pd/MnO₂ catalysts. (b) Effect of reaction time on selectivity and FA conversion over Pd/Co₃O₄ catalysts. Reaction conditions: FA = 0.5 g, isopropanol = 20 mL, catalyst = 10 mg, H₂ = 20 bar, reaction temperature = 180 °C, and stirring speed = 600 rpm.

Based on these results, we found that Pd/Co₃O₄ catalysts selectively produced MF as a major secondary product via the hydrogenolysis of the C–O bond of FA, which was generated from FAL. It was confirmed that the yield of FA was dominant at an initial stage of the FAL hydrogenation over the Pd/Co₃O₄ catalyst. When the production of FA was maximized, it then decreased at the expense of MF production. It was obvious that a much higher yield of MF was observed, when FA was used as a feed over Pd/Co₃O₄ instead of FAL. However, over the Pd/MnO₂ catalyst, FA was the main reaction product, at which aldehyde hydrogenation toward FA was the preferred reaction pathway for the conversion of FAL. Therefore, when FA was used as a feed, very low activity was observed on the Pd/MnO₂ catalyst, indicating that the secondary hydrogenolysis to MF from FA did not occur (Fig. 8a). The extraordinary enhancement of the reaction rate and the changes in selectivity over Pd/Co₃O₄ compared to other Pd/oxides are illustrated in Scheme 1. FAL was hydrogenated to FA on the Pd surface, followed by the secondary hydrogenolysis to MF from FA at the interface between Pd and Co₃O₄ oxide. For the other Pd/oxide catalysts such as Pd/MnO₂, only FAL hydrogenation to FA occurs dominantly on the Pd surface.



Scheme 1. Illustration showing potential reaction sites and reaction pathways over Pd/Co₃O₄ and Pd/MnO₂ catalysts during FAL hydrogenation.

4. Conclusion

The highly dispersed Pd NPs deposited on mesoporous oxides of Co₃O₄, MnO₂, NiO, CeO₂, and Fe₂O₃ were prepared via the nanocasting and chemical reduction method for the development of efficient catalysts for liquid-phase FAL hydrogenation. While mesoporous oxides show a trace amount of catalytic activity in FAL hydrogenation, Pd/oxide catalysts greatly enhance the catalytic conversions of FAL depending on the type of mesoporous oxides. The change in support affects the Pd dispersion as well as the redox behavior of Pd species which strongly influence the catalytic activity and selectivity in the FAL hydrogenation. Pd/Co₃O₄, Pd/MnO₂, and Pd/NiO possess a high Pd dispersion, resulting in a high FAL conversion, while low conversions are observed in Pd/CeO₂ and Pd/Fe₂O₃ catalysts owing to their poor Pd dispersion. In the product selectivity, the Pd/Co₃O₄ catalyst induces predominant production of MF via hydrogenolysis, while other Pd/oxide catalysts prefer the reaction pathway via the aldehyde hydrogenation, yielding FA as the major product. In the hydrogenation of FA instead of FAL, it is revealed that MF as a secondary product is derived from FA via the hydrogenolysis of C–O over the Pd/Co₃O₄ catalyst, rather than direct formation from FAL. As a result, FAL is hydrogenated to FA preferentially on the Pd surface, and then the secondary hydrogenolysis to MF from FA is further promoted at the interface between Pd and Co₃O₄. This reaction pathway is totally different from that of Pd/MnO₂, which produces FA dominantly. It is also demonstrated that Pd/Fe₂O₃ shows unusual interfacial behaviors due to the remaining surfactants, which cover the active site of Pd, resulting in a low conversion of FAL. Because the characteristics of the mesoporous oxides determine the Pd-oxide interfaces

in the current study, a proper selection of the support facilitates a high catalytic conversion of desired products in many biomass conversions.

Associated content

Supplementary Materials

Author Information

Declaration of interests

The authors declare that they have no known competing financial interests or personal relationships that could have appeared to influence the work reported in this paper.

The authors declare the following financial interests/personal relationships which may be considered as potential competing interests:

Acknowledgements

This research was supported by Basic Science Research Program (2018R1A1A1A05079555) and Technology Development Program to Solve Climate Changes (2017M1A2A2087630) of the National Research Foundation of Korea (NRF) funded by the Ministry of Science and ICT, and MOTIE (KIAT_N0001754) and UNIST (1.180082.01).

References

- [1] R.R. Davda, J.W. Shabaker, G.W. Huber, R.D. Cortright, J.A. Dumesic, *Appl. Catal. B-Environ.* 56 (2005) 171-186.
- [2] D. Sutton, B. Kelleher, J.R.H. Ross, *Fuel Process. Technol.* 73 (2001) 155-173.
- [3] J.Y. Park, L.R. Baker, G.A. Somorjai, *Chem. Rev.* 115 (2015) 2781-2817.
- [4] **M.A. Banares, *Catal. Today* 51 (1999) 319-348.**
- [5] G.W. Huber, S. Iborra, A. Corma, *Chem. Rev.* 106 (2006) 4044-4098.
- [6] J. Zakzeski, P.C.A. Bruijninx, A.L. Jongerius, B.M. Weckhuysen, *Chem. Rev.* 110 (2010) 3552-3599.
- [7] P. Munnik, P.E. de Jongh, K.P. de Jong, *Chem. Rev.* 115 (2015) 6687-6718.
- [8] Y. Hu, X.J. Yang, S. Cao, J.E. Zhou, Y.X. Wu, J.Y. Han, Z.G. Yan, M.M. Zheng, *Appl. Surf. Sci.*, 400 (2017) 148-153.
- [9] M. Comotti, W.C. Li, B. Spliethoff, F. Schuth, *J. Am. Chem. Soc.*, 128 (2006) 917-924.
- [10] Q. Fu, T. Wagner, *Surf. Sci. Rep.*, 62 (2007) 431-498.
- [11] M.M. Schubert, S. Hackenberg, A.C. van Veen, M. Muhler, V. Plzak, R.J. Behm, *J. Catal.*, 197 (2001) 113-122.
- [12] K. An, S. Alayoglu, N. Musselwhite, S. Plamthottam, G. Melaet, A.E. Lindeman, G.A. Somorjai, *J. Am. Chem. Soc.*, 135 (2013) 16689-16696.
- [13] C. Nguyen-Huy, J.S. Kim, S. Yoon, E. Yang, J.H. Kwak, M.S. Lee, K. An, *Fuel*, 226 (2018) 607-617.
- [14] I.X. Green, W.J. Tang, M. Neurock, J.T. Yates, *Science*, 333 (2011) 736-739.
- [15] L.F. Yang, S.Y. Shan, R. Loukrakpam, V. Petkov, Y. Ren, B.N. Wanjala, M.H. Engelhard, J. Luo, J. Yin, Y.S. Chen, C.J. Zhong, *J. Am. Chem. Soc.*, 134 (2012) 15048-15060.
- [16] A.R. Puigdollers, P. Schlexer, S. Tosoni, G. Pacchioni, *Acs Catal.*, 7 (2017) 6493-6513.
- [17] G.F. Zhao, F. Yang, Z.J. Chen, Q.F. Liu, Y.J. Ji, Y. Zhang, Z.Q. Niu, J.J. Mao, X.H. Bao, P.J. Hu, Y.D. Li, *Nat. Commun.*, 8 (2017).
- [18] J. Graciani, K. Mudiyansele, F. Xu, A.E. Baber, J. Evans, S.D. Senanayake, D.J. Stacchiola, P. Liu, J. Hrbek, J.F. Sanz, J.A. Rodriguez, *Science*, 345 (2014) 546-550.
- [19] X.Q. Wang, J.A. Rodriguez, J.C. Hanson, D. Gamarra, A. Martinez-Arias, M. Fernandez-Garcia, *J. Phys. Chem. B*, 110 (2006) 428-434.
- [20] J.B. Park, J. Graciani, J. Evans, D. Stacchiola, S.D. Senanayake, L. Barrio, P. Liu, J.F. Sanz, J. Hrbek, J.A. Rodriguez, *J. Am. Chem. Soc.*, 132 (2010) 356-363.
- [21] W.Q. Xu, R. Si, S.D. Senanayake, J. Llorca, H. Idriss, D. Stacchiola, J.C. Hanson, J.A. Rodriguez, *J. Catal.*, 291 (2012) 117-126.
- [22] L.Q. Liu, F. Zhou, L.G. Wang, X.J. Qi, F. Shi, Y.Q. Deng, *J. Catal.*, 274 (2010) 1-10.
- [23] A. Abad, P. Concepcion, A. Corma, H. Garcia, *Angew Chem. Int. Edit.*, 44 (2005) 4066-4069.
- [24] E.A. Redina, A.A. Greish, I.V. Mishin, G.I. Kapustin, O.P. Tkachenko, O.A. Kirichenko, L.M. Kustov, *Catal. Today*, 241 (2015) 246-254.
- [25] S.J. Tauster, S.C. Fung, R.T.K. Baker, J.A. Horsley, *Science*, 211 (1981) 1121-1125.
- [26] A.B. Boffa, C. Lin, A.T. Bell, G.A. Somorjai, *Catal. Lett.*, 27 (1994) 243-249.
- [27] A. Bruix, J.A. Rodriguez, P.J. Ramirez, S.D. Senanayake, J. Evans, J.B. Park, D. Stacchiola, P. Liu, J. Hrbek, F. Illas, *J. Am. Chem. Soc.*, 134 (2012) 8968-8974.
- [28] L.R. Baker, G. Kennedy, M. Van Spronsen, A. Hervier, X.J. Cai, S.Y. Chen, L.W. Wang, G.A. Somorjai, *J. Am. Chem. Soc.*, 134 (2012) 14208-14216.

- [29] J. Kijenski, P. Winiarek, T. Paryjczak, A. Lewicki, A. Mikolajska, *Appl. Catal. a-Gen.*, 233 (2002) 171-182.
- [30] G.W. Huber, S. Iborra, A. Corma, *Chem. Rev.*, 106 (2006) 4044-4098.
- [31] J.N. Chheda, G.W. Huber, J.A. Dumesic, *Angew Chem. Int. Edit.*, 46 (2007) 7164-7183.
- [32] G.W. Huber, J.N. Chheda, C.J. Barrett, J.A. Dumesic, *Science*, 308 (2005) 1446-1450.
- [33] C.J. Barrett, J.N. Chheda, G.W. Huber, J.A. Dumesic, *Appl. Catal. B-Environ.*, 66 (2006) 111-118.
- [34] V. Choudhary, S.I. Sandler and D.G. Vlachos, *Acs Catal.*, 2 (2012) 2022-2028.
- [35] R. Mariscal, P. Maireles-Torres, M. Ojeda, I. Sadaba, M.L. Granados, *Energ. Environ. Sci.*, 9 (2016) 1144-1189.
- [36] A. Mandalika, T. Runge, *Green. Chem.*, 14 (2012) 3175-3184.
- [37] M. Besson, P. Gallezot, C. Pinel, *Chem. Rev.*, 114 (2014) 1827-1870.
- [38] P. Maki-Arvela, B. Holmbom, T. Salmi, D.Y. Murzin, *Catal. Rev.*, 49 (2007) 197-340.
- [39] G.Y. Li, N. Li, S.S. Li, A.Q. Wang, Y. Cong, X.D. Wang, T. Zhang, *Chem. Commun.*, 49 (2013) 5727-5729.
- [40] J.P. Lange, E. van der Heide, J. van Buijtenen, R. Price, *Chemsuschem*, 5 (2012) 150-166.
- [41] M.F. Fellah, *Appl. Surf. Sci.*, 405 (2017) 395-404.
- [42] Y. Roman-Leshkov, C.J. Barrett, Z.Y. Liu, J.A. Dumesic, *Nature*, 447 (2007) 982-U985.
- [43] E. Christensen, J. Yanowitz, M. Ratcliff, R.L. McCormick, *Energ. Fuel*, 25 (2011) 4723-4733.
- [44] N. Xu, C.L. Tang, X. Meng, X.S. Fan, Z.M. Tian, Z.H. Huang, *Energ. Fuel*, 29 (2015) 5372-5381.
- [45] E. Christensen, G.M. Fioroni, S. Kim, L. Fouts, E. Gjersing, R.S. Paton, R.L. McCormick, *Fuel*, 212 (2018) 576-585.
- [46] M. Thewes, M. Muether, S. Pischinger, M. Budde, A. Brunn, A. Sehr, P. Adomeit, J. Kankermayer, *Energ. Fuel*, 25 (2011) 5549-5561.
- [47] K. Xiong, W.T. Yu, J.G.G. Chen, *Appl. Surf. Sci.*, 323 (2014) 88-95.
- [48] Y. Nakagawa, H. Nakazawa, H. Watanabe, K. Tomishige, *Chemcatchem*, 4 (2012) 1791-1797.
- [49] P. Panagiotopoulou, D.G. Vlachos, *Appl. Catal. a-Gen.*, 480 (2014) 17-24.
- [50] S. Sitthisa, T. Pham, T. Prasomsri, T. Sooknoi, R.G. Mallinson, D.E. Resasco, *J. Catal.*, 280 (2011) 17-27.
- [51] V. Vorotnikov, G. Mpourmpakis, D.G. Vlachos, *Acs Catal.*, 2 (2012) 2496-2504.
- [52] Shit, S. C., Singuru, R., Pollastri, S., Joseph, B., Rao, B. S., Lingaiah, N., & Mondal, J., *Catal. Sci. Technol.*, 8 (2018) 2195-2210
- [53] Sarkar, C., Koley, P., Shown, I., Lee, J., Liao, Y. F., An, K., ... & Mondal, J., *ACS Sustainable Chem. Eng.* 7 (2019) 10349-10362
- [54] Singuru, R., Dhanalaxmi, K., Shit, S. C., Reddy, B. M., & Mondal, J., *ChemCatChem* 9 (2017) 2550-2564
- [55] C. Jo, K. Kim, R. Ryoo, *Micropor. Mesopor. Mat.*, 124 (2009) 45-51.
- [56] R.M. Rioux, H. Song, J.D. Hoefelmeyer, P. Yang, G.A. Somorjai, *J. Phys. Chem. B*, 109 (2005) 2192-2202.
- [57] A. Taguchi, F. Schuth, *Micropor. Mesopor. Mat.*, 77 (2005) 1-45.
- [58] A.H. Lu, F. Schuth, *Adv. Mater.*, 18 (2006) 1793-1805.
- [59] Y. Ren, Z. Ma, L.P. Qian, S. Dai, H.Y. He, P.G. Bruce, *Catal. Lett.*, 131 (2009) 146-154.

- [60] M. Mihaylov, H. Knozinger, K. Hadjiivanov, B.C. Gates, *Chem.-Ing.-Tech.*, 79 (2007) 795-806.
- [61] H. Jeong, J. Bae, J.W. Han, H. Lee, *Acs Catal.*, 7 (2017) 7097-7105.
- [62] J. Szanyi, J.H. Kwak, *Phys. Chem. Chem. Phys.*, 16 (2014) 15126-15138.
- [63] S. Sasidharan, A. Jayasree, S. Fazal, M. Koyakutty, S.V. Nair, D. Menon, *Biomater. Sci.-Uk*, 1 (2013) 294-305.
- [64] J. Lee, J. Woo, C. Nguyen-Huy, M.S. Lee, K. An, *Catal. Today* (2009) in press.

Journal Pre-proof